

Linear scaling relation between two-dimensional massless Dirac fermion Fermi velocity and Fe-As bond length in iron arsenide superconductor systems

Chengpu Lv,^{1,2} Jianzhou Zhao³, Yueshan Xu,^{1,2} Yu Song⁴, Chenglin Zhang,⁴ Mykhaylo Ozerov⁵, Pengcheng Dai⁴, Nan-Lin Wang⁶, and Zhi-Guo Chen (湛志国)^{1,7,*}

¹Beijing National Laboratory for Condensed Matter Physics, Institute of Physics, Chinese Academy of Sciences, Beijing 100190, China

²School of Physical Sciences, University of Chinese Academy of Sciences, Beijing 100190, China

³Co-Innovation Center for New Energetic Materials, Southwest University of Science and Technology, Mianyang, Sichuan 621010, China

⁴Department of Physics and Astronomy, Rice University, Houston, Texas 77005, USA

⁵National High Magnetic Field Laboratory, Tallahassee, Florida 32310, USA

⁶International Center for Quantum Materials, School of Physics, Peking University, Beijing 100871, China

⁷Songshan Lake Materials Laboratory, Dongguan, Guangdong 523808, China

 (Received 29 December 2024; revised 29 April 2025; accepted 21 May 2025; published 12 June 2025)

Two-dimensional (2D) massless Dirac fermions (MDF), which represent a type of quasiparticles with linear energy-momentum dispersions only in 2D momentum space, provide a fertile ground for realizing novel quantum phenomena. However, 2D MDF were seldom observed in the superconducting bulk states of 3D materials. Furthermore, as a cornerstone for accurately tuning the quantum phenomena based on 2D MDF, a quantitative relationship between 2D MDF and a structural parameter has rarely been revealed so far. Here, we report magnetoinfrared spectroscopy studies of the iron-arsenide-superconductor systems NaFeAs and AFe₂As₂ (A = Ca, Ba) at temperature $T \sim 4.2$ K and at magnetic fields (B) up to 17.5 T. Our results demonstrate the existence of 2D MDF in the superconducting bulk state of NaFeAs. Moreover, the 2D-MDF Fermi velocities in NaFeAs and AFe₂As₂ (A = Ca, Ba), which are extracted from the slopes of the linear \sqrt{B} dependences of the Landau-level transition energies, scale linearly with the Fe-As bond lengths. The linear scaling between the 2D-MDF Fermi velocities and the Fe-As bond lengths is supported by (i) the linear relationship between the square root of the effective mass of the d_{xy} electrons and the Fe-As bond length and (ii) the linear dependence of the square root of the calculated tight-binding hopping energy on the Fe-As bond length. Our results open up avenues for exploring and tuning quantum phenomena based on 2D MDF in the superconducting bulk states of 3D materials.

DOI: [10.1103/143s-hq6d](https://doi.org/10.1103/143s-hq6d)

Two-dimensional (2D) massless Dirac fermions (MDF) in condensed matter have attracted enormous interest due to their crucial roles in achieving various exotic quantum phenomena, which include novel quantum Hall effect [1–3], Klein tunneling [4], and giant linear magnetoresistance [5]. Noteworthy, a large part of quantum phenomena based on 2D MDF can be largely influenced by the 2D-MDF Fermi velocity [6,7]. Thus a scaling relation concerning 2D-MDF Fermi velocity can serve as an important basis for accurately tuning the related quantum phenomena. Previously, 2D-MDF Fermi velocity was mostly revealed to have the quantitative relationships with the physical quantities depicting electron-electron interactions [6,7]. However, the scaling between 2D-MDF Fermi velocity and a quantity concerning the other degree of freedom remains elusive. Furthermore, most of the 2D MDF were observed on the surfaces of 3D topological insulators and in 2D materials, e.g., graphene [8–12]. Few 3D materials host 2D MDF in their bulk.

Previous investigations indicated that, in the antiferromagnetic (AFM) bulk states of 3D iron-arsenide-superconductor systems [see Fig. 1(a)] [13,14], the paramagnetic-Brillouin-zone folding results in the crossing points of the linearly

dispersing bands, which are *topologically protected* by the AFM order, inversion symmetry and a combination of time-reversal and spin-reversal symmetry, emerges near Fermi energy (E_F) [see Fig. 1(b)] [15–31]. In addition, angle-resolved photoemission spectroscopy (ARPES) studies showed that linear band dispersions within the $k_x - k_y$ plane are present below E_F in the low-temperature AFM bulk state of iron-arsenide-superconductor systems [17,23,27,28]. Therefore, MDF with linear energy-momentum dispersions and topologically protected band-crossing points are present in the AFM bulk states of iron-arsenide-superconductor systems [15–22,24–26]. However, to date, only “122”-type iron arsenides have been identified both experimentally and theoretically to possess topologically nontrivial 2D MDF in their AFM bulk [29]. 2D MDF have yet been observed in the superconducting bulk states of 3D iron-arsenide-superconductor systems. A natural question to ask is whether a broader system of iron-arsenide superconductors can be found to have topologically nontrivial 2D MDF in the bulk state. Moreover, a scaling relationship about the 2D-MDF Fermi velocity in iron-arsenide-superconductor systems, which is expected to be significant for tuning exotic quantum phenomena based on their 2D MDF, is still lacking.

Topologically nontrivial 2D MDF have been discovered on the surfaces of iron-based superconductors [32–34]. More

*Contact author: zgchen@iphy.ac.cn

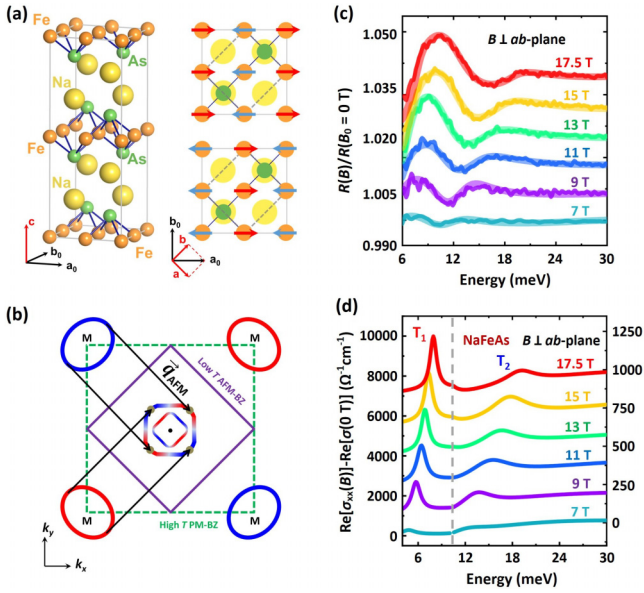


FIG. 1. Antiferromagnetic (AFM) order, Fermi surfaces, and magneto-optical response of NaFeAs. (a) Left: orthorhombic unit cell of NaFeAs in the AFM state, containing two FeAs layers. Right: collinear AFM order in two FeAs layers. The dashed and solid gray lines display the paramagnetic (PM) unit cell within the FeAs layer at high temperatures and the unit cell after the AFM phase transition, respectively. (b) Schematic of the Fermi surfaces of NaFeAs in the PM state. Four node (i.e., Dirac) points (gray dots) and Dirac cones emerge after the folding of the PM BZ along the AFM wave vector (the black arrows). (c) Relative reflectance spectra $R(B)/R(B_0 = 0 \text{ T})$ of NaFeAs at different magnetic fields. The solid curves with noise and the partially transparent curves in (c) represent the measured $R(B)/R(B_0 = 0 \text{ T})$ spectra of NaFeAs and the magneto-optical fits to the measured spectra, respectively. (d) Relative real part of the optical conductivity of NaFeAs. The $R(B)/R(B_0 = 0 \text{ T})$ spectra in (c) and the T_1 peak and the T_2 peak in (d) are displaced from one another by 0.009, 1400 ($\Omega^{-1}\text{cm}^{-1}$), and 200 ($\Omega^{-1}\text{cm}^{-1}$) for clarity, respectively

importantly, owing to the proximity effect from the superconducting bulk, a superconducting gap would be opened in the topologically nontrivial 2D MDF state, which can induce topological superconductivity on the surfaces of iron-based superconductors [35–38]. As a key feature of topological superconductivity, Majorana zero modes have been reported to emerge inside the vortex cores of the superconducting surfaces of iron-based superconductors, which offers a potential platform for realizing topological quantum computing [39–43]. It is worth noticing that, at ambient pressure, 3D iron-arsenide superconductor NaFeAs with the superconducting transition temperature $T_c \sim 23 \text{ K}$ exhibits an AFM order below 39 K, which (i) means that an AFM order and superconductivity coexist in the bulk ground state of NaFeAs and (ii) implies that 2D MDF may be present in its superconducting bulk state. More importantly, searching for topologically nontrivial 2D MDF in the superconducting bulk state of NaFeAs is expected to provide a crucial clue to exploring quantum phenomena including topological superconductivity [44–48]. Nonetheless, whether 2D MDF exist in the superconducting bulk state of NaFeAs is still unclear.

Magnetoinfrared spectroscopy is a bulk-sensitive experimental technique for investigating 2D MDF [49,50] in materials as it can probe the Landau level (LL) transitions of 2D MDF. Here, we performed the magnetoinfrared spectroscopy measurements of the single crystals of NaFeAs and CaFe_2As_2 at $T \sim 4.2 \text{ K}$ with the applied magnetic field parallel to the wave vector of the incident light and the crystalline c axis (see the details about the single-crystal growth and magnetoinfrared measurements in Sec. S1 of the Supplemental Material [51]). Figure 1(c) displays the relative reflectance spectra $R(B)/R(B_0 = 0 \text{ T})$ of NaFeAs measured at different magnetic fields. Peaklike features are present in the $R(B)/R(B_0 = 0 \text{ T})$ and systematically move towards higher energies as the magnetic field is enhanced. To identify the nature of the peaklike features in the $R(B)/R(B_0 = 0 \text{ T})$, we obtained the real part of the diagonal optical conductivity $\text{Re}[\sigma_{xx}(B, \omega)]$ by fitting the absolute reflectance spectra $R(B)$ based on the magneto-optical model (see the details about the fitting based on the magneto-optical model in Sec. S2 of the Supplemental Material [51] and see also Refs. [52,53] therein). In Fig. 1(d), the peaklike features can be observed in the relative optical conductivity spectra $\text{Re}[\sigma_{xx}(B, \omega)] - \text{Re}[\sigma(B = 0 \text{ T}, \omega)]$ of NaFeAs. Considering that (i) the highest magnetic field ($B_{\text{max}} = 17.5 \text{ T}$) applied along the crystalline c axis here is much lower than that ($B > 500 \text{ T}$) for dramatically destroying the AFM order in iron-arsenide-superconductor systems at low temperatures [54] and (ii) the energy region ($\sim 30 \text{ meV}$) where the peaklike features are present in Fig. 1(d) is narrower than the energy region ($\sim 100 \text{ meV}$) where the spectral weight is transferred due to the AFM phase transition in NaFeAs [55], the observed peaklike features in the $R(B)/R(B_0 = 0 \text{ T})$ and the $\text{Re}[\sigma_{xx}(B, \omega)] - \text{Re}[\sigma(B = 0 \text{ T}, \omega)]$ here are irrelevant with the magnetic-field-induced change in the AFM order of NaFeAs. Furthermore, the direction of the magnetic field here is perpendicular to that (orthorhombic a or b axis) of the magnetic field used for partially detwinning the single crystals of iron-arsenide superconductor systems [56–58], so the peaklike features in Figs. 1(c) and 1(d) are unlikely to arise from the detwinning.

To further study the origin of the observed peaklike features in the superconducting and AFM state of NaFeAs, we plotted the energies of the peaklike features in the $\text{Re}[\sigma_{xx}(B, \omega)] - \text{Re}[\sigma(B = 0 \text{ T}, \omega)]$ spectra as a function of \sqrt{B} in Fig. 2(a), which shows that the energies (i.e., E_{T_1} and E_{T_2}) of the two peaklike features T_1 and T_2 not only exhibit a linear dependence on \sqrt{B} and the zero intercepts at $B = 0 \text{ T}$ under linear extrapolations but also have the ratio $E_{T_2}/E_{T_1} \approx 2.4$. Therein, the \sqrt{B} dependences of the T_1 and T_2 energies provide a signature of the fermions with linear energy-momentum dispersions. Moreover, the zero intercepts at $B = 0 \text{ T}$ under the linear extrapolations of the T_1 and T_2 energies indicate that the energy gap between the linearly dispersing valence and conduction bands is zero (i.e., the presence of band-degeneracy points) and that the corresponding fermions have zero mass. Thus the \sqrt{B} dependence of the peak energy positions transition energies and the zero-energy intercepts at $B = 0 \text{ T}$ manifest the existence of massless fermions with linear dispersions and band-degeneracy points in the superconducting and AFM bulk state of NaFeAs.

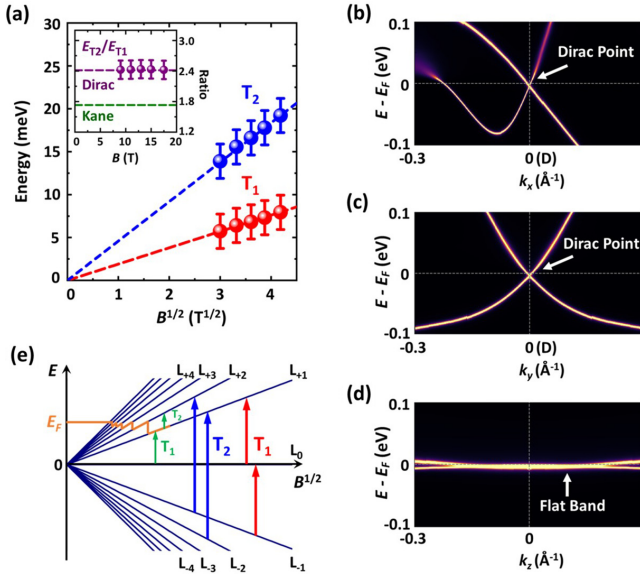


FIG. 2. Landau level transitions and band dispersions of NaFeAs in the AFM state. (a) Observed two LL transitions, T_1 and T_2 , in an $E - \sqrt{B}$ plot. The inset shows energy ratio of the two LL transitions as a function of B . The purple and green dashed lines show the theoretical energy ratios which are based on massless Dirac and Kane models, respectively. (b)–(d) Calculated band dispersions of NaFeAs along k_x , k_y , and k_z near E_F . The flat band in (d) represents the energy-momentum dispersion of MDF along k_z in NaFeAs. (e) Schematic of the LL transitions of 2D MDF in NaFeAs. The magnetic field dependence of the assumed Fermi level is shown by the orange lines. The two green arrows indicate the assumed T_1 and T_2 in case (i).

In condensed matter, there are mainly three kinds of massless fermions with linear dispersions and band-degeneracy points, which include MDF, Kane fermions, and Weyl fermions [1–3, 59–64]. For Kane fermions, the maximal energy ratio among their adjacent LLs is $\sqrt{3/2} : \sqrt{1/2} \approx 1.732$, which is distinctly *smaller* than that between the observed T_2 and T_1 [see the inset of Fig. 2(a)]. Additionally, previous theoretical studies showed that the flat band of Kane fermions is absent around the band-degeneracy point of the linearly dispersing bands of iron-arsenide-superconductor systems [15, 16]. Thus the observed peaklike features in the $R(B)/R(B_0 = 0 \text{ T})$ and the $\text{Re}[\sigma_{xx}(B, \omega)] - \text{Re}[\sigma(B = 0 \text{ T}, \omega)]$ spectra of NaFeAs are very unlikely to be contributed by the optical transitions between the LLs of Kane fermions (see the discussion in Sec. S3 of the Supplemental Material [51] and see also references [59, 60] therein). For Weyl fermions, their lowest-energy peaklike feature arising from the zeroth-LL-related inter-LL transition $\text{LL}_{-1} \rightarrow \text{LL}_{\pm 0}$ (or $\text{LL}_{\pm 0} \rightarrow \text{LL}_{+1}$) in the $\text{Re}[\sigma_{xx}(B)] - \text{Re}[\sigma(0 \text{ T})]$ spectra should be *weaker* than the second lowest-energy peaklike feature induced by the inter-LL transition $\text{LL}_{-1} \rightarrow \text{LL}_{+2}$ or ($\text{LL}_{-2} \rightarrow \text{LL}_{+1}$) [65, 66] (see the discussion in Sec. S3 of the Supplemental Material [51]), which is on the contrary to the case of NaFeAs shown in Fig. 1(d). Besides, previous theoretical studies showed that the degenerate nodal points in iron-arsenide-superconductor systems have the same chirality [15, 16], which is in contrast to the opposite chirality of a

pair of Weyl nodes [61–64]. Therefore, the observed peaklike features in Figs. 1(c) and 1(d) should be irrelevant with the optical transitions between the LLs of Weyl fermions. Based on the above discussion, we assign the peaklike features in the magneto-optical spectra of NaFeAs to the LL transitions of MDF.

For 2D MDF, the lowest energy peak feature of the zeroth-LL-related inter-LL transition $\text{LL}_{-1} \rightarrow \text{LL}_{\pm 0}$ (or $\text{LL}_{\pm 0} \rightarrow \text{LL}_{+1}$) in $\text{Re}[\sigma_{xx}(B)] - \text{Re}[\sigma(0 \text{ T})]$ is stronger than the second lowest-energy peak feature of the inter-LL transition $\text{LL}_{-1} \rightarrow \text{LL}_{+2}$ (or $\text{LL}_{-2} \rightarrow \text{LL}_{+1}$) because of a singularity of the density of state (DOS) of the zeroth LLs of 2D Dirac fermions [29, 65, 66], which is consistent with the relative intensity between the peaklike features T_1 and T_2 in Fig. 1(d), while, for 3D MDF, the lowest-energy peak feature of the zeroth-LL related inter-LL transition $\text{LL}_{-1} \rightarrow \text{LL}_{\pm 0}$ (or $\text{LL}_{\pm 0} \rightarrow \text{LL}_{+1}$) in $\text{Re}[\sigma_{xx}(B)] - \text{Re}[\sigma(0 \text{ T})]$ is *weaker* than the second lowest-energy peak feature of the inter-LL transition $\text{LL}_{-1} \rightarrow \text{LL}_{+2}$ or ($\text{LL}_{-2} \rightarrow \text{LL}_{+1}$) due to the absence of a DOS singularity of the zeroth LLs of 3D MDF [65], which is similar to the case for Weyl fermions. Thus the dominance of the peaklike feature T_1 in the $\text{Re}[\sigma_{xx}(B)] - \text{Re}[\sigma(0 \text{ T})]$ indicates that MDF in the superconducting and AFM bulk state of NaFeAs should be 2D. Besides, in Figs. 2(b)–2(d), our DFT + DMFT calculations show that, in the superconducting and AFM state of NaFeAs, the bands near E_F disperse linearly along the k_x and k_y directions, but disperse quite weakly along the k_z direction (see the details about the calculations in Sec. S1 of the Supplemental Material [51] and see also Refs. [67–70] therein), which further supports 2D MDF in this iron-arsenide superconductor.

The LL spectrum of 2D MDF without considering Zeeman effects can be given by [29, 49, 50]

$$E_n^{2D} = \text{sgn}(n) v_F^D \sqrt{2e\hbar|n|B}, \quad (1)$$

where v_F^D is the 2D-MDF Fermi velocity, the integer n is LL index, $\text{sgn}(n)$ is the sign function, e is the elementary charge, and \hbar is Planck's constant divided by 2π . Given the selection rule for the allowed optical transitions from LL_n to $\text{LL}_{n'}$ [29, 49, 50]

$$\Delta n = |n| - |n'| = \pm 1, \quad (2)$$

the energies $E_{n \rightarrow n'}^{2D}$ of the allowed optical transitions from LL_n to $\text{LL}_{n'}$ have the form

$$E_{n \rightarrow n'}^{2D} = v_F^D \sqrt{B} [\text{sgn}(n') \sqrt{2e\hbar|n'|} - \text{sgn}(n) \sqrt{2e\hbar|n|}]. \quad (3)$$

According to Eqs. (1) and (3), two groups of LL transitions of 2D MDF have the energy ratios which are close to that (~ 2.4) between T_2 and T_1 : (i) the energy ratio $1 : (\sqrt{2} - 1) \approx 2.414$ between the LL transitions, $\text{LL}_{-1} \rightarrow \text{LL}_0$ and $\text{LL}_{-2} \rightarrow \text{LL}_{-1}$ (or $\text{LL}_0 \rightarrow \text{LL}_{+1}$ and $\text{LL}_{+1} \rightarrow \text{LL}_{+2}$) and (ii) the energy ratio $(1 + \sqrt{2}) : 1 \approx 2.414$ between the LL transitions, $\text{LL}_{-1} \rightarrow \text{LL}_{+2}$ and $\text{LL}_{-1} \rightarrow \text{LL}_0$ (or $\text{LL}_{-2} \rightarrow \text{LL}_{+1}$ and $\text{LL}_0 \rightarrow \text{LL}_{+1}$). To extract the 2D-MDF Fermi velocity in NaFeAs, it is essential to determine which group of LL transitions of 2D MDF leads to the two peaklike features T_1 and T_2 . If we assumed that the peaklike features T_1 and T_2 separately arise from the LL transitions $\text{LL}_{-2} \rightarrow \text{LL}_{-1}$ and $\text{LL}_{-1} \rightarrow \text{LL}_0$ (or $\text{LL}_{+1} \rightarrow \text{LL}_{+2}$ and $\text{LL}_0 \rightarrow \text{LL}_{+1}$) [see the two green arrows in Fig. 2(e)], the E_F should be still

pinned on LL_{+1} or LL_{-1} at $B = 17.5$ T due to the presence of the intra-LL transition $LL_{-2} \rightarrow LL_{-1}$ (or $LL_{+1} \rightarrow LL_{+2}$). Considering (i) the 2D-MDF Fermi velocity obtained based on Eq. (3), $v_F^D \approx 1.30 \times 10^5$ m/s, and (ii) the LL_{+1} (or LL_{-1}) energy calculated at $B = 17.5$ T based on Eq. (1), the corresponding E_F in NaFeAs is about 81 meV, which is much higher than the experimental E_F of ~ 2 meV measured by ARPES and the theoretical E_F of ~ 3 meV gotten by our DFT + DMFT calculations. Moreover, as the magnetic field increases, electrons in LL_{+1} (or holes in LL_{-1}) would be depopulated, which would lead to the decrease in the spectral weight of the lowest-energy absorption feature resulting from the assumed LL transition $LL_{-2} \rightarrow LL_{-1}$ (or $LL_{+1} \rightarrow LL_{+2}$). In contrast, the lowest-energy peaklike feature T_1 in the $\text{Re}[\sigma_{xx}(B, \omega)] - \text{Re}[\sigma(B = 0 \text{ T}, \omega)]$ of NaFeAs becomes more dominant with increasing the magnetic field. Thus the measured peaklike features T_1 and T_2 should not arise from the LL transitions in case (i): $LL_{-1} \rightarrow LL_0$ and $LL_{-2} \rightarrow LL_{-1}$ (or $LL_0 \rightarrow LL_{+1}$ and $LL_{+1} \rightarrow LL_{+2}$). For case (ii), the observation of the peaklike feature T_1 which is assumed to come from the LL transition $LL_{-1} \rightarrow LL_0$ (or $LL_0 \rightarrow LL_{+1}$) at $B \leq 9$ T suggests that NaFeAs enters the quantum limit at low magnetic fields [71,72], which is in agreement with the low E_F measured by ARPES [24]. Moreover, in case (ii), based on Eq. (3), the obtained 2D-MDF Fermi velocity $v_F^D \approx 5.4 \times 10^4$ m/s, which is comparable to the values deduced from the ARPES results. Thus the peaklike features T_1 and T_2 in the $\text{Re}[\sigma_{xx}(B, \omega)] - \text{Re}[\sigma(B = 0 \text{ T}, \omega)]$ of NaFeAs should be assigned to the LL transitions, $LL_{-1} \rightarrow LL_{+2}$ and $LL_{-1} \rightarrow LL_0$ (or $LL_{-2} \rightarrow LL_{+1}$ and $LL_0 \rightarrow LL_{+1}$), respectively, which corresponds to the $v_F^D \approx 5.4 \times 10^4$ m/s.

To check whether 2D MDF exist in the bulk state of iron arsenide CaFe_2As_2 , we performed the DFT + DMFT calculations on its electronic bands (see the details about the calculations in Sec. S1 of the Supplemental Material [51] and see also Refs. [67–70] therein). In Figs. 3(a)–3(c), our DFT + DMFT calculations exhibit the linear band dispersions along k_x and k_y directions and the very weak dispersions along k_z direction, which indicates that CaFe_2As_2 possesses 2D MDF as well. To obtain the 2D-MDF Fermi velocity in CaFe_2As_2 , we measured its relative reflectance spectra $R(B)/R(B_0 = 0 \text{ T})$ at different magnetic fields [see the clear peaklike feature in each $R(B)/R(B_0 = 0 \text{ T})$ spectrum in Fig. 3(d) and each $R(B)/R(B_0 = 0 \text{ T})$ spectrum down to 6 meV in Fig. S4] and got its $\text{Re}[\sigma_{xx}(B, \omega)] - \text{Re}[\sigma(B = 0 \text{ T}, \omega)]$ spectra via fitting the $R(B)$ [see Fig. 3(e) and the fitting parameters in Tables S1–S14 of the Supplemental Material [51]]. The energy region (~ 45 meV) where the peaklike features are present in the relative optical conductivity spectra of CaFe_2As_2 in Fig. 3(e) is narrower than not only the energy region (up to at least 207 meV) where the spectral weight is transferred due to its AFM phase transition but also the energy (~ 82 meV) of its small spin-density-wave gap [73], which indicates that the observed peaklike features in the relative reflectance spectra and the relative optical conductivity spectra of CaFe_2As_2 are unlikely to be relevant with the magnetic-field-induced change in its AFM order. Moreover, the energy position of the peaklike feature in Fig. 4(a) shows a linear dependence on \sqrt{B} and has the zero-energy intercept at $B = 0$ T under the linear extrapolation as well, which suggests that the peaklike feature

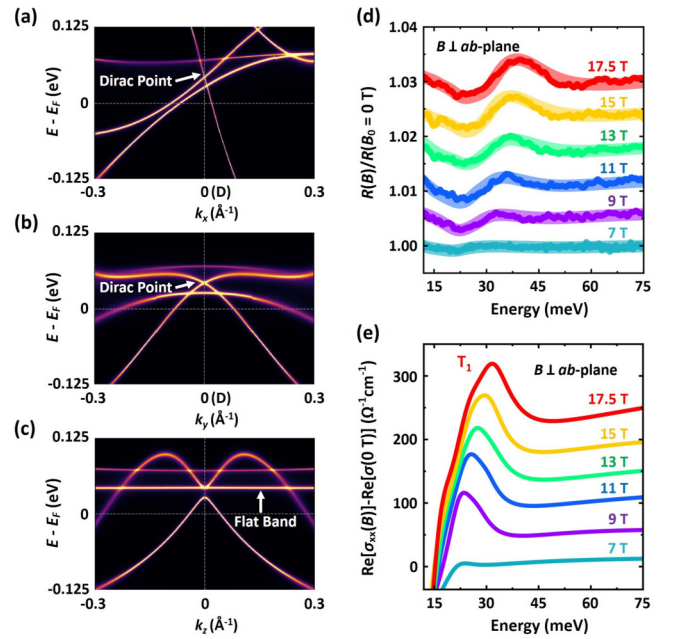


FIG. 3. Magneto-optical response and band dispersions of CaFe_2As_2 in the AFM state. (a)–(c) Calculated energy-momentum dispersions of MDF in CaFe_2As_2 along k_x , k_y , and k_z . The flat band in (c) represents the energy-momentum dispersion of MDF along k_z in CaFe_2As_2 . (d) Relative reflectance spectra $R(B)/R(B_0 = 0 \text{ T})$ of CaFe_2As_2 . The solid curves with noise and the partially transparent curves in (d) represent the measured $R(B)/R(B_0 = 0 \text{ T})$ spectra of CaFe_2As_2 and the magneto-optical fits to the measured spectra, respectively. (e) Relative optical conductivity spectra of CaFe_2As_2 . The spectra in (d) and (e) are separately displaced from one another by 0.006 and 50 ($\Omega^{-1}\text{cm}^{-1}$) for clarity.

arises from the LL transition of 2D MDF. Given that (i) the E_F obtained by our DFT + DMFT calculations is low and (ii) the spectral weight of the peaklike feature is enhanced with the growth of the magnetic field, the peaklike feature in Fig. 3(d) can be ascribed to the lowest-energy LL transition $LL_{-1} \rightarrow LL_0$ (or $LL_0 \rightarrow LL_{+1}$) of 2D MDF. Then, we fitted the linear \sqrt{B} dependence of the peak energy position based on Eq. (3) and obtained the derived 2D-MDF Fermi velocity $v_F^D \approx 2.16 \times 10^5$ m/s. The 2D-MDF Fermi velocity in CaFe_2As_2 is larger than those in NaFeAs and BaFe_2As_2 ($v_F^D \approx 1.18 \times 10^4$ m/s) [29], which is consistent with the fact that the peaklike feature in the relative optical conductivity spectra of CaFe_2As_2 at $B = 17.5$ T is located at the highest energy position among those of NaFeAs and AFe_2As_2 ($A = \text{Ba}, \text{Ca}$) here.

The increase in the 2D-MDF Fermi velocity from NaFeAs to AFe_2As_2 ($A = \text{Ba}, \text{Ca}$) inspires us to search for the relation between the 2D-MDF Fermi velocities and lattice parameters. Thus we plotted the Fe-As-distance and As-Fe-As-angle dependences of the 2D-MDF Fermi velocities of NaFeAs, BaFe_2As_2 , and CaFe_2As_2 , respectively [see Fig. 4(b), Fig. S2, and the Fe-As distance and the As-Fe-As angle in Fig. 2(a) of Ref. [48]]. The quantitative relation between the 2D-MDF Fermi velocities and the As-Fe-As angles seems to be elusive (see Fig. S2). However, interestingly, the 2D-MDF Fermi velocities in NaFeAs, BaFe_2As_2 , and

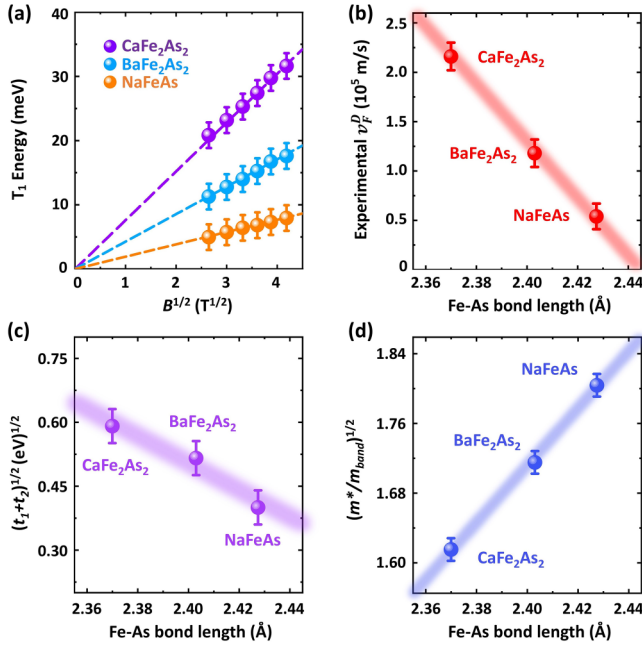


FIG. 4. Relationship between the 2D-MDF Fermi velocities and the Fe-As bond lengths in NaFeAs, BaFe₂As₂, and CaFe₂As₂. (a) \sqrt{B} dependences of the T₁ energies of NaFeAs, BaFe₂As₂, and CaFe₂As₂. (b) Linear scaling between the 2D-MDF Fermi velocities and the Fe-As bond lengths. (c) Linear relationship between $\sqrt{t_1(xy, xy) + t_2(xy, xy)}$ and the Fe-As bond lengths [48]. (d) Linear scaling between $\sqrt{m^*/m_{\text{band}}}$ and the Fe-As bond lengths [48]. m_{band} is the band mass.

CaFe₂As₂ scale linearly with the Fe-As bond lengths which are the quantities about lattice degree of freedom [see Fig. 4(b)]. Previous DFT + DMFT calculations showed that the Dirac cones of iron-arsenide-superconductor systems near E_F are mainly composed of iron d_{xy} orbital [74]. For iron-arsenide-superconductor systems, the shorter Fe-As distance suggests more overlap between the Fe-3d and As-4p orbitals, which means an easier hopping of the d_{xy} electrons occupying the Dirac cone and thus implies a larger bandwidth (W). For 2D MDF with linear dispersions in iron-arsenide-superconductor systems, the larger bandwidth within the same momentum range (Δk) corresponds to the higher 2D-MDF Fermi velocity due to the relationship $v_F^D = W/\Delta k$.

To check the linear scaling between the 2D-MDF Fermi velocities and the Fe-As bond lengths in NaFeAs, BaFe₂As₂, and CaFe₂As₂, we further studied the kinetic energy (E_k) and the effective mass (m^*) of the d_{xy} electrons because the Dirac cones near E_F are dominated by iron d_{xy} orbital. In a low-energy effective tight-binding model, the hopping parameters (t) can be approximately regarded to be proportional to the kinetic energy E_k , so we plotted the square root of the sum of the DFT + DMFT-calculation-derived tight-binding hopping parameters [$t_1(xy, xy)$ and $t_2(xy, xy)$] for the electrons on the iron d_{xy} orbital hopping to the orbital d_{xy} of their nearest neighbor and next nearest neighbor iron atoms, i.e., $\sqrt{t_1(xy, xy) + t_2(xy, xy)}$ for NaFeAs, BaFe₂As₂, and CaFe₂As₂ with different Fe-As bond lengths in Fig. 4(c) [see the $t_1(xy, xy)$ and $t_2(xy, xy)$ in Fig. S5 of the Supplemental Material of Ref. [48]]. The $\sqrt{t_1(xy, xy) + t_2(xy, xy)}$ shows a

linear relationship with the Fe-As bond length. The square root of the effective mass m^* of the d_{xy} electrons in Fig. 1(b) of Ref. [48] exhibits a linear dependence on the Fe-As bond length as well [see Fig. 4(d)]. Considering the linear relationship for “relativistic” fermions in solids $v_F^D = \sqrt{E_k/m^*}$, the 2D-MDF Fermi velocities in NaFeAs, BaFe₂As₂, and CaFe₂As₂ should scale linearly with the Fe-As bond lengths.

In summary, our observation of the \sqrt{B} dependence of the LL transition energies, the zero-energy intercept at $B = 0$ T under linear extrapolations of the transition energies, the energy ratio (~ 2.4) between the two LL transitions, and the dominant absorption features of the zeroth-LL-related transitions, together with the DFT + DMFT-calculation-derived linear band dispersions in 2D momentum space, demonstrate that 2D MDF exist in the superconducting bulk state of NaFeAs. In addition, the LL transition energy of CaFe₂As₂ displays the linear \sqrt{B} dependence and the zero-energy intercept at $B = 0$ T. Moreover, the 2D-MDF Fermi velocities in NaFeAs, BaFe₂As₂, and CaFe₂As₂, which are extracted from the slopes of the linear \sqrt{B} dependences of the LL transition energies, increase linearly with the Fe-As bond lengths—quantities about lattice degree of freedom. The linear scaling between the 2D-MDF Fermi velocities and the Fe-As bond lengths is supported by (i) the linear dependence of the $\sqrt{m^*}$ of the d_{xy} electrons on the Fe-As bond length and (ii) the linear scaling between the $\sqrt{t_1(xy, xy) + t_2(xy, xy)}$ and the Fe-As bond length. Our work offers a material platform hosting both 2D MDF and superconductivity in the 3D bulk for discovering and tuning exotic quantum phenomena.

We thank Z. Yin, Z. Li, M. Orlita, Y. Ran, O. Vafek, and P. Richard for very helpful discussions. The authors acknowledge support from the Guangdong Basic and Applied Basic Research Foundation (Project No. 2021B1515130007), the strategic Priority Research Program of Chinese Academy of Sciences (Project No. XDB33000000), the National Natural Science Foundation of China (Grant No. U21A20432), the National Key Research and Development Program of China (Grant No. 2022YFA1403800), and the Synergetic Extreme Condition User Facility (SECUF [75])–Infrared Unit in THz and Infrared Experimental Station. The single-crystal growth and characterization efforts at Rice are supported by the U.S. Department of Energy, Office of Basic Energy Sciences, under Award No. DE-SC0012311 (P.D.). A portion of this work was performed in NHMFL, which is supported by National Science Foundation Cooperative Agreement No. DMR-1157490 and the State of Florida.

C.L., J.Z., and Y.X. contributed equally to this work. Z.-G.C. conceived and supervised this project. Y.S., C.Z., and P.D. grew the single crystals; N.-L.W. performed the infrared studies at zero magnetic field; Z.-G.C. carried out the magnetoinfrared experiments; partial magnetoinfrared measurements were performed in NHMFL with the assistance from M.O.; J.Z. did the DFT + DMFT calculations; Z.-G.C., C.L., and Y.X. analyzed the data; Z.-G.C. wrote the paper with the input from C.L.

The data that support the findings of this article are not publicly available. The data are available from the authors upon reasonable request.

- [1] K. S. Novoselov, A. K. Geim, S. V. Morozov, D. Jiang, Y. Zhang, S. V. Dubonos, I. V. Grigorieva, and A. A. Firsov, Electric field effect in atomically thin carbon films, *Science* **306**, 666 (2004).
- [2] K. S. Novoselov, A. K. Geim, S. V. Morozov, D. Jiang, M. I. Katsnelson, I. V. Grigorieva, S. V. Dubonos, and A. A. Firsov, Two-dimensional gas of massless Dirac fermions in graphene, *Nature (London)* **438**, 197 (2005).
- [3] Y. Zhang, Y.-W. Tan, H. L. Stormer, and P. Kim, Experimental observation of the quantum Hall effect and Berry's phase in graphene, *Nature (London)* **438**, 201 (2005).
- [4] C. W. J. Beenakker, Colloquium: Andreev reflection and Klein tunneling in graphene, *Rev. Mod. Phys.* **80**, 1337 (2008).
- [5] T. Liang, Q. Gibson, M. N. Ali, M. Liu, R. J. Cava, and N. P. Ong, Ultrahigh mobility and giant magnetoresistance in the Dirac semimetal Cd_3As_2 , *Nat. Mater.* **14**, 280 (2015).
- [6] D. C. Elias, R. V. Gorbachev, A. S. Mayorov, S. V. Morozov, A. A. Zhukov, P. Blake, L. A. Ponomarenko, I. V. Grigorieva, K. S. Novoselov, F. Guinea, and A. K. Geim, Dirac cones reshaped by interaction effects in suspended graphene, *Nat. Phys.* **7**, 701 (2011).
- [7] C. Faugeras, S. Berciaud, P. Leszczynski, Y. Henni, K. Nogajewski, M. Orlita, T. Taniguchi, K. Watanabe, C. Forsythe, P. Kim, R. Jalil, A. K. Geim, D. M. Basko, and M. Potemski, Landau level spectroscopy of electron-electron interactions in graphene, *Phys. Rev. Lett.* **114**, 126804 (2015).
- [8] Y. Feng, D. Liu, B. Feng, X. Liu, L. Zhao, Z. Xie, Y. Liu, A. Liang, C. Hu, Y. Hu, S. He, G. Liu, J. Zhang, C. Chen, Z. Xu, L. Chen, K. Wu, Y.-T. Liu, H. Lin, Z.-Q. Huang *et al.*, Direct evidence of interaction-induced Dirac cones in a monolayer silicene/Ag(111) system, *Proc. Natl. Acad. Sci. USA* **113**, 14656 (2016).
- [9] D. Hsieh, D. Qian, L. Wray, Y. Xia, Y. S. Hor, R. J. Cava, and M. Z. Hasan, A topological Dirac insulator in a quantum spin Hall phase, *Nature (London)* **452**, 970 (2008).
- [10] Y. L. Chen, J. G. Analytis, J.-H. Chu, Z. K. Liu, S.-K. Mo, X. L. Qi, H. J. Zhang, D. H. Lu, X. Dai, Z. Fang, S. C. Zhang, I. R. Fisher, Z. Hussain, and Z.-X. Shen, Experimental Realization of a Three-Dimensional Topological Insulator, Bi_2Te_3 , *Science* **325**, 178 (2009).
- [11] P. Cheng, C. Song, T. Zhang, Y. Zhang, Y. Wang, J.-F. Jia, J. Wang, Y. Wang, B.-F. Zhu, X. Chen, X. Ma, K. He, L. Wang, X. Dai, Z. Fang, X. Xie, X.-L. Qi, C.-X. Liu, S.-C. Zhang, and Q.-K. Xue, Landau quantization of topological surface states in Bi_2Se_3 , *Phys. Rev. Lett.* **105**, 076801 (2010).
- [12] T. Hanaguri, K. Igarashi, M. Kawamura, H. Takagi, and T. Sasagawa, Momentum-resolved Landau-level spectroscopy of Dirac surface state in Bi_2Se_3 , *Phys. Rev. B* **82**, 081305(R) (2010).
- [13] Q. Huang, Y. Qiu, W. Bao, M. A. Green, J. W. Lynn, Y. C. Gasparovic, T. Wu, G. Wu, and X. H. Chen, Neutron-diffraction measurements of magnetic order and a structural transition in the parent BaFe_2As_2 compound of FeAs-Based high-temperature superconductors, *Phys. Rev. Lett.* **101**, 257003 (2008).
- [14] J. Zhao, W. Ratcliff, J. W. Lynn, G. F. Chen, J. L. Luo, N. L. Wang, J. Hu, and P. Dai, Spin and lattice structures of single-crystalline SrFe_2As_2 , *Phys. Rev. B* **78**, 140504(R) (2008).
- [15] Y. Ran, F. Wang, H. Zhai, A. Vishwanath, and D.-H. Lee, Nodal spin density wave and band topology of the FeAs-based materials, *Phys. Rev. B* **79**, 014505 (2009).
- [16] T. Morinari, E. Kaneshita, and T. Tohyama, Topological and transport properties of dirac fermions in an antiferromagnetic metallic phase of iron-based superconductors, *Phys. Rev. Lett.* **105**, 037203 (2010).
- [17] P. Richard, K. Nakayama, T. Sato, M. Neupane, Y. M. Xu, J. H. Bowen, G. F. Chen, J. L. Luo, N. L. Wang, X. Dai, Z. Fang, H. Ding, and T. Takahashi, Observation of Dirac cone electronic dispersion in BaFe_2As_2 , *Phys. Rev. Lett.* **104**, 137001 (2010).
- [18] N. Harrison and S. E. Sebastian, Dirac nodal pockets in the antiferromagnetic parent phase of FeAs superconductors, *Phys. Rev. B* **80**, 224512 (2009).
- [19] M. Nakajima, T. Liang, S. Ishida, Y. Tomioka, K. Kihou, C. H. Lee, A. Iyo, H. Eisaki, T. Kakeshita, T. Ito, and S. Uchida, Unprecedented anisotropic metallic state in undoped iron arsenide BaFe_2As_2 revealed by optical spectroscopy, *Proc. Natl. Acad. Sci. USA* **108**, 12238 (2011).
- [20] K. K. Huynh, Y. Tanabe, and K. Tanigaki, Both electron and hole Dirac cone states in $\text{Ba}(\text{FeAs})_2$ confirmed by magnetoresistance, *Phys. Rev. Lett.* **106**, 217004 (2011).
- [21] T. Terashima, N. Kurita, M. Tomita, K. Kihou, C.-H. Lee, Y. Tomioka, T. Ito, A. Iyo, H. Eisaki, T. Liang, M. Nakajima, S. Ishida, S.-I. Uchida, H. Harima, and S. Uji, Complete fermi surface in BaFe_2As_2 observed via shubnikov-de haas oscillation measurements on detwinned single crystals, *Phys. Rev. Lett.* **107**, 176402 (2011).
- [22] M. Matusiak, Z. Bukowski, and J. Karpinski, Doping dependence of the Nernst effect in $\text{Eu}(\text{Fe}_{1-x}\text{Co}_x)_2\text{As}_2$: Departure from Dirac-fermion physics, *Phys. Rev. B* **83**, 224505 (2011).
- [23] C. He, Y. Zhang, B. P. Xie, X. F. Wang, L. X. Yang, B. Zhou, F. Chen, M. Arita, K. Shimada, H. Namatame, M. Taniguchi, X. H. Chen, J. P. Hu, and D. L. Feng, Electronic-structure-driven magnetic and structure transitions in superconducting NaFeAs single crystals measured by angle-resolved photoemission spectroscopy, *Phys. Rev. Lett.* **105**, 117002 (2010).
- [24] M. Yi, D. H. Lu, R. G. Moore, K. Kihou, C. H. Lee, A. Iyo, H. Eisaki, T. Yoshida, A. Fujimori, and Z. X. Shen, Electronic reconstruction through the structural and magnetic transitions in detwinned NaFeAs, *New J. Phys.* **14**, 073019 (2012).
- [25] S. Sugai, Y. Mizuno, R. Watanabe, T. Kawaguchi, K. Takenaka, H. Ikuta, Y. Takayanagi, N. Hayamizu, and Y. Sone, Spin-Density-Wave gap with dirac nodes and two-magnon raman scattering in BaFe_2As_2 , *J. Phys. Soc. Jpn.* **81**, 024718 (2012).
- [26] Y. Imai, F. Nabeshima, D. Nakamura, T. Katase, H. Hiramatsu, H. Hosono, and A. Maeda, Ultralow-Dissipative conductivity by dirac fermions in BaFe_2As_2 , *J. Phys. Soc. Jpn.* **82**, 043709 (2013).
- [27] S. Y. Tan, Y. Fang, D. H. Xie, W. Feng, C. H. P. Wen, Q. Song, Q. Y. Chen, W. Zhang, Y. Zhang, L. Z. Luo, B. P. Xie, X. C. Lai, and D. L. Feng, Observation of Dirac cone band dispersions in FeSe thin films by photoemission spectroscopy, *Phys. Rev. B* **93**, 104513 (2016).
- [28] S. V. Bakurskiy, N. V. Klenov, I. I. Soloviev, M. Y. Kupriyanov, and A. A. Golubov, Superconducting phase domains for memory applications, *Appl. Phys. Lett.* **108**, 042602 (2016).
- [29] Z.-G. Chen, L. Wang, Y. Song, X. Lu, H. Luo, C. Zhang, P. Dai, Z. Yin, K. Haule, and G. Kotliar, Two-Dimensional

- massless Dirac fermions in antiferromagnetic $A\text{Fe}_2\text{As}_2$ ($A = \text{Ba}, \text{Sr}$), *Phys. Rev. Lett.* **119**, 096401 (2017).
- [30] T. Terashima, H. T. Hirose, D. Graf, Y. Ma, G. Mu, T. Hu, K. Suzuki, S. Uji, and H. Ikeda, Fermi surface with Dirac fermions in CaFeAsF determined via quantum oscillation measurements, *Phys. Rev. X* **8**, 011014 (2018).
- [31] B. Xu, H. Xiao, B. Gao, Y. H. Ma, G. Mu, P. Marsik, E. Shevelova, F. Lyzwa, Y. M. Dai, R. P. S. M. Lobo, and C. Bernhard, Optical study of Dirac fermions and related phonon anomalies in the antiferromagnetic compound CaFeAsF , *Phys. Rev. B* **97**, 195110 (2018).
- [32] F. Wang and D.-H. Lee, Topological relation between bulk gap nodes and surface bound states: Application to iron-based superconductors, *Phys. Rev. B* **86**, 094512 (2012).
- [33] A. Lau and C. Timm, Topological surface states and Andreev bound states in superconducting iron pnictides, *Phys. Rev. B* **90**, 024517 (2014).
- [34] P. Zhang, Z. Wang, X. Wu, K. Yaji, Y. Ishida, Y. Kohama, G. Dai, Y. Sun, C. Bareille, K. Kuroda, T. Kondo, K. Okazaki, K. Kindo, X. Wang, C. Jin, J. Hu, R. Thomale, K. Sumida, S. Wu, K. Miyamoto *et al.*, Multiple topological states in iron-based superconductors, *Nat. Phys.* **15**, 41 (2019).
- [35] Z. Wang, P. Zhang, G. Xu, L. K. Zeng, H. Miao, X. Xu, T. Qian, H. Weng, P. Richard, A. V. Fedorov, H. Ding, X. Dai, and Z. Fang, Topological nature of the $\text{FeSe}_{0.5}\text{Te}_{0.5}$ superconductor, *Phys. Rev. B* **92**, 115119 (2015).
- [36] G. Xu, B. Lian, P. Tang, X.-L. Qi, and S.-C. Zhang, Topological superconductivity on the surface of Fe-based superconductors, *Phys. Rev. Lett.* **117**, 047001 (2016).
- [37] P. Zhang, K. Yaji, T. Hashimoto, Y. Ota, T. Kondo, K. Okazaki, Z. Wang, J. Wen, G. D. Gu, H. Ding, and S. Shin, Observation of topological superconductivity on the surface of an iron-based superconductor, *Science* **360**, 182 (2018).
- [38] S. Qin, C. Fang, F.-C. Zhang, and J. Hu, Topological superconductivity in an extended s -Wave superconductor and its implication to iron-based superconductors, *Phys. Rev. X* **12**, 011030 (2022).
- [39] D. Wang, L. Kong, P. Fan, H. Chen, S. Zhu, W. Liu, L. Cao, Y. Sun, S. Du, J. Schneeloch, R. Zhong, G. Gu, L. Fu, H. Ding, and H.-J. Gao, Evidence for Majorana bound states in an iron-based superconductor, *Science* **362**, 333 (2018).
- [40] R.-X. Zhang, W. S. Cole, and S. Das Sarma, Helical hinge majorana modes in iron-based superconductors, *Phys. Rev. Lett.* **122**, 187001 (2019).
- [41] K. Jiang, X. Dai, and Z. Wang, Quantum anomalous vortex and Majorana zero mode in iron-based superconductor $\text{Fe}(\text{Te}, \text{Se})$, *Phys. Rev. X* **9**, 011033 (2019).
- [42] Z. Wang, J. O. Rodriguez, L. Jiao, S. Howard, M. Graham, G. D. Gu, T. L. Hughes, D. K. Morr, and V. Madhavan, Evidence for dispersing 1D Majorana channels in an iron-based superconductor, *Science* **367**, 104 (2020).
- [43] W. Liu, L. Cao, S. Zhu, L. Kong, G. Wang, M. Papaj, P. Zhang, Y.-B. Liu, H. Chen, G. Li, F. Yang, T. Kondo, S. Du, G.-H. Cao, S. Shin, L. Fu, Z. Yin, H.-J. Gao, and H. Ding, A new Majorana platform in an Fe-As bilayer superconductor, *Nat. Commun.* **11**, 5688 (2020).
- [44] C.-H. Lee, A. Iyo, H. Eisaki, H. Kito, M. T. Fernandez-Diaz, T. Ito, K. Kihou, H. Matsuhata, M. Braden, and K. Yamada, Effect of structural parameters on superconductivity in fluorine-free LnFeAsO_{1-y} ($\text{Ln} = \text{La}, \text{Nd}$), *J. Phys. Soc. Jpn.* **77**, 083704 (2008).
- [45] Y. Mizuguchi, Y. Hara, K. Deguchi, S. Tsuda, T. Yamaguchi, K. Takeda, H. Kotegawa, H. Tou, and Y. Takano, Anion height dependence of T_c for the Fe-based superconductor, *Supercond. Sci. Technol.* **23**, 054013 (2010).
- [46] H. Okabe, N. Takeshita, K. Horigane, T. Muranaka, and J. Akimitsu, Pressure-induced high- T_c superconducting phase in FeSe : Correlation between anion height and T_c , *Phys. Rev. B* **81**, 205119 (2010).
- [47] D. C. Johnston, The puzzle of high temperature superconductivity in layered iron pnictides and chalcogenides, *Adv. Phys.* **59**, 803 (2010).
- [48] Z. P. Yin, K. Haule, and G. Kotliar, Kinetic frustration and the nature of the magnetic and paramagnetic states in iron pnictides and iron chalcogenides, *Nat. Mater.* **10**, 932 (2011).
- [49] M. L. Sadowski, G. Martinez, M. Potemski, C. Berger, and W. A. de Heer, Landau level spectroscopy of ultrathin graphite layers, *Phys. Rev. Lett.* **97**, 266405 (2006).
- [50] Z. Jiang, E. A. Henriksen, L. C. Tung, Y. J. Wang, M. E. Schwartz, M. Y. Han, P. Kim, and H. L. Stormer, Infrared spectroscopy of Landau levels of graphene, *Phys. Rev. Lett.* **98**, 197403 (2007).
- [51] See Supplemental Material at <http://link.aps.org/supplemental/10.1103/143s-hq6d> for the single-crystal growth, infrared reflectance measurements, DFT+DMFT calculations, detailed methods for obtaining the relative real part of the optical conductivity, and optical transitions between the Landau levels of Kane fermions and Weyl fermions, which also contains Refs. [29,52,53,59,60,67–70].
- [52] E. D. Palik and J. K. Furdyna, Infrared and microwave magnetoplasma effects in semiconductors, *Rep. Prog. Phys.* **33**, 1193 (1970).
- [53] B. Su, Y. Song, Y. Hou, X. Chen, J. Zhao, Y. Ma, Y. Yang, J. Guo, J. Luo, and Z.-G. Chen, Strong and Tunable electrical anisotropy in type-II Weyl semimetal candidate WP_2 with broken inversion symmetry, *Adv. Mater.* **31**, 1903498 (2019).
- [54] M. Tokunaga, I. Katakura, N. Katayama, and K. Ohgushi, High-field studies on single crystals of EuFe_2As_2 , *J. Low Temp. Phys.* **159**, 601 (2010).
- [55] W. Z. Hu, G. Li, P. Zheng, G. F. Chen, J. L. Luo, and N. L. Wang, Optical study of the spin-density-wave properties of single-crystalline $\text{Na}_{1-\delta}\text{FeAs}$, *Phys. Rev. B* **80**, 100507(R) (2009).
- [56] M. A. Tanatar, A. Kreyssig, S. Nandi, N. Ni, S. L. Bud'ko, P. C. Canfield, A. I. Goldman, and R. Prozorov, Direct imaging of the structural domains in the iron pnictides $A\text{Fe}_2\text{As}_2$ ($A = \text{Ca}, \text{Sr}, \text{Ba}$), *Phys. Rev. B* **79**, 180508(R) (2009).
- [57] J.-H. Chu, J. G. Analytis, D. Press, K. De Greve, T. D. Ladd, Y. Yamamoto, and I. R. Fisher, In-plane electronic anisotropy in underdoped $\text{Ba}(\text{Fe}_{1-x}\text{Co}_x)_2\text{As}_2$ revealed by partial detwinning in a magnetic field, *Phys. Rev. B* **81**, 214502 (2010).
- [58] S. Zapf, C. Stingl, K. W. Post, J. Maiwald, N. Bach, I. Pietsch, D. Neubauer, A. Löhle, C. Clauss, S. Jiang, H. S. Jeevan, D. N. Basov, P. Gegenwart, and M. Dressel, Persistent detwinning of iron-pnictide EuFe_2As_2 crystals by small external magnetic fields, *Phys. Rev. Lett.* **113**, 227001 (2014).

- [59] M. Orlita, D. M. Basko, M. S. Zholudev, F. Tepe, W. Knap, V. I. Gavrilenko, N. N. Mikhailov, S. A. Dvoretiskii, P. Neugebauer, C. Faugeras, A. L. Barra, G. Martinez, and M. Potemski, Observation of three-dimensional massless Kane fermions in a zinc-blende crystal, *Nat. Phys.* **10**, 233 (2014).
- [60] F. Tepe, M. Marcinkiewicz, S. S. Krishtopenko, S. Ruffenach, C. Consejo, A. M. Kadykov, W. Desrat, D. But, W. Knap, J. Ludwig, S. Moon, D. Smirnov, M. Orlita, Z. Jiang, S. V. Morozov, V. I. Gavrilenko, N. N. Mikhailov, and S. A. Dvoretiskii, Temperature-driven massless Kane fermions in HgCdTe crystals, *Nat. Commun.* **7**, 12576 (2016).
- [61] H. Weng, C. Fang, Z. Fang, B. A. Bernevig, and X. Dai, Weyl semimetal phase in noncentrosymmetric transition-metal monophosphides, *Phys. Rev. X* **5**, 011029 (2015).
- [62] S.-Y. Xu, C. Liu, S. K. Kushwaha, R. Sankar, J. W. Krizan, I. Belopolski, M. Neupane, G. Bian, N. Alidoust, T.-R. Chang, H.-T. Jeng, C.-Y. Huang, W.-F. Tsai, H. Lin, P. P. Shibayev, F.-C. Chou, R. J. Cava, and M. Z. Hasan, Observation of Fermi arc surface states in a topological metal, *Science* **347**, 294 (2015).
- [63] B. Q. Lv, N. Xu, H. M. Weng, J. Z. Ma, P. Richard, X. C. Huang, L. X. Zhao, G. F. Chen, C. E. Matt, F. Bisti, V. N. Strocov, J. Mesot, Z. Fang, X. Dai, T. Qian, M. Shi, and H. Ding, Observation of Weyl nodes in TaAs, *Nat. Phys.* **11**, 724 (2015).
- [64] L. X. Yang, Z. K. Liu, Y. Sun, H. Peng, H. F. Yang, T. Zhang, B. Zhou, Y. Zhang, Y. F. Guo, M. Rahn, D. Prabhakaran, Z. Hussain, S. K. Mo, C. Felser, B. Yan, and Y. L. Chen, Weyl semimetal phase in the non-centrosymmetric compound TaAs, *Nat. Phys.* **11**, 728 (2015).
- [65] P. E. C. Ashby and J. P. Carbotte, Magneto-optical conductivity of Weyl semimetals, *Phys. Rev. B* **87**, 245131 (2013).
- [66] Y. Sun and A.-M. Wang, Magneto-optical conductivity of double Weyl semimetals, *Phys. Rev. B* **96**, 085147 (2017).
- [67] K. Haule, C.-H. Yee, and K. Kim, Dynamical mean-field theory within the full-potential methods: Electronic structure of CeIrIn₅, CeCoIn₅, and CeRhIn₅, *Phys. Rev. B* **81**, 195107 (2010).
- [68] P. Blaha, K. Schwarz, F. Tran, R. Laskowski, G. K. H. Madsen, and L. D. Marks, WIEN2k: An APW+lo program for calculating the properties of solids, *J. Chem. Phys.* **152**, 074101 (2020).
- [69] E. Gull, A. J. Millis, A. I. Lichtenstein, A. N. Rubtsov, M. Troyer, and P. Werner, Continuous-time Monte Carlo methods for quantum impurity models, *Rev. Mod. Phys.* **83**, 349 (2011).
- [70] K. Haule, Exact double counting in combining the dynamical mean field theory and the density functional theory, *Phys. Rev. Lett.* **115**, 196403 (2015).
- [71] M. Orlita, C. Faugeras, J. M. Schneider, G. Martinez, D. K. Maude, and M. Potemski, Graphite from the viewpoint of Landau level spectroscopy: An effective graphene bilayer and monolayer, *Phys. Rev. Lett.* **102**, 166401 (2009).
- [72] M. Orlita, I. Crassee, C. Faugeras, A. B. Kuzmenko, F. Fromm, M. Ostler, Th. Seyller, G. Martinez, M. Polini, and M. Potemski, Classical to quantum crossover of the cyclotron resonance in graphene: a study of the strength of intraband absorption, *New J. Phys.* **14**, 095008 (2012).
- [73] Y. M. Dai, A. Akrap, S. L. Bud'ko, P. C. Canfield, and C. C. Homes, Optical properties of AFe₂As₂ (A = Ca, Sr, and Ba) single crystals, *Phys. Rev. B* **94**, 195142 (2016).
- [74] Z. P. Yin, K. Haule, and G. Kotliar, Magnetism and charge dynamics in iron pnictides, *Nat. Phys.* **7**, 294 (2011).
- [75] <https://cstr.cn/31123.02.SECUF>.